



OPEN ACCESS

EDITED BY

Yunlong Huo,
Shanghai Jiao Tong University, China

REVIEWED BY

Aike Qiao,
Beijing University of Technology, China
Fan Tingting,
Capital Medical University, China

*CORRESPONDENCE

Yuehong Zheng,
✉ zhengyuehong2022@outlook.com
Xiao Liu,
✉ liuxiao@buaa.edu.cn

†These authors have contributed equally to this work and share first authorship

SPECIALTY SECTION

This article was submitted to Computational Physiology and Medicine, a section of the journal Frontiers in Physiology

RECEIVED 02 December 2022

ACCEPTED 28 December 2022

PUBLISHED 10 January 2023

CITATION

Sun X, Li S, He Y, Liu Y, Ma T, Zeng R, Liu Z, Chen Y, Zheng Y and Liu X (2023), Effects of cardiac function alterations on the risk of postoperative thrombotic complications in patients receiving endovascular aortic repair. *Front. Physiol.* 13:1114110. doi: 10.3389/fphys.2022.1114110

COPYRIGHT

© 2023 Sun, Li, He, Liu, Ma, Zeng, Liu, Chen, Zheng and Liu. This is an open-access article distributed under the terms of the [Creative Commons Attribution License \(CC BY\)](https://creativecommons.org/licenses/by/4.0/). The use, distribution or reproduction in other forums is permitted, provided the original author(s) and the copyright owner(s) are credited and that the original publication in this journal is cited, in accordance with accepted academic practice. No use, distribution or reproduction is permitted which does not comply with these terms.

Effects of cardiac function alterations on the risk of postoperative thrombotic complications in patients receiving endovascular aortic repair

Xiaoning Sun^{1,2†}, Siting Li^{1,2†}, Yuan He^{3†}, Yuxi Liu^{3†}, Tianxiang Ma³, Rong Zeng¹, Zhili Liu¹, Yu Chen³, Yuehong Zheng^{1,2*} and Xiao Liu^{3*}

¹Department of Vascular Surgery, Peking Union Medical College Hospital, Chinese Academy of Medical Sciences, Peking Union Medical College, Beijing, China, ²Department, State Key Laboratory of Complex Severe and Rare Diseases, Peking Union Medical College Hospital, Chinese Academy of Medical Science and Peking Union Medical College, Beijing, China, ³Key Laboratory of Biomechanics and Mechanobiology, Ministry of Education, Beijing Advanced Innovation Center for Biomedical Engineering, School of Biological Science and Medical Engineering, Beihang University, Beijing, China

Introduction: Chronic heart disease (CHD) is a common comorbidity of patients receiving endovascular aneurysm repair (EVAR) for abdominal aortic aneurysms (AAA). The explicit relationship between ventricular systolic function and EVAR complication of thrombotic events is unknown.

Methods: In this study, we proposed a three-dimensional numerical model coupled with the lumped-elements heart model, which is capable of simulating thrombus formation in diverse systolic functions. The relation of cardiac functions and the predicted risk of thrombus formation in the aorta and/or endograft of 4 patients who underwent EVAR was investigated. Relative risks for thrombus formation were identified using machine-learning algorithms.

Results: The computational results demonstrate that thrombus tended to form on the interior side of the aorta arch and iliac branches, and cardiac function can affect blood flow field and affect thrombus formation, which is consistent with the four patients' post-operative imaging follow-up. We also found that RRT, OSI, TAWSS in thrombosis area are lower than whole average. In addition, we found that the thrombus formation has negative correlations with the maximum ventricular contractile force ($r = -.281 \pm .101$) and positive correlations with the minimum ventricular contractile force ($r = .238 \pm .074$), whereas the effect of heart rate ($r = -.015 \pm .121$) on thrombus formation is not significant.

Conclusion: In conclusion, changes in ventricular systolic function may alter the risk of thrombotic events after EVAR repair, which could provide insight into the selection of adjuvant therapy strategies for AAA patients with CHD.

KEYWORDS

thrombus, hemodynamics, computational model, ventricular systolic function, abdominal aortic aneurysms

Introduction

Abdominal aortic aneurysm (AAA) is one of the most common degenerative aortic diseases and is often complicated with various levels of cardiac dysfunction and cardiovascular comorbidities (Lim et al., 2015). For advanced and/or rapid-growing aneurysms, prompt surgical or endovascular interventions are indicated, among which endovascular aortic aneurysm repair (EVAR) is widely accepted as the first-line treatment option for anatomically feasible cases (Isselbacher et al., 2022). Cardiac comorbidities may increase the risk of perioperative surgical complications and affect mid-to-long-term prognosis (Khashram et al., 2016). Levels of cardiac function and functional reserve determine the quality of the patients' tolerance to surgical interventions and the efficacy of postoperative rehabilitation.

Intraluminal thrombus formation is commonly observed not only in major arteries with atherosclerotic and aneurysmal lesions but also, to a lesser degree, intra-prosthetically after endovascular stenting. Despite its lower rate of occurrence, intra-prosthetic thrombus formation may lead to post-operative distal embolism, branch occlusion, and critical end-organ malperfusion (Maleux et al., 2008; Perini et al., 2018; Banno et al., 2021). The formation of intraluminal thrombus and thrombogenic atherosclerotic plaques are believed to be driven by hemodynamic factors. Pathogenic blood flow that generates oscillatory and non-physiological wall shear stress may trigger the accumulation of lipid and pro-thrombotic factors (Cunningham and Gotlieb, 2005). Furthermore, postoperative hemodynamic alterations in the aorta and its major branches are largely determined by the extent of cardiac response and anatomic modifications (Pagoulatou et al., 2021). Individual cardiac functions vary among patients of different ages and physical conditions. However, quantitative data of cardiac functions (cardiac output, stroke volume, etc.) is often unavailable because the measuring process may not be regularly included in the standard protocol of preoperative clinical assessment in real-world scenarios. We noted that only limited and contradicted evidence exists on whether peri- and postoperative use of cardiac supportive drugs such as β -blockers could be beneficial for AAA patients after EVAR in light of aneurysmal sac shrinking and clinical outcomes (Saratzis et al., 2008; Kim et al., 2017; Salata et al., 2018). The effects of variations in cardiac function on the risk of intraluminal and intra-prosthetic thrombus formation are yet to be further elaborated.

By modeling the process of hemodynamics and mass transport in the coagulation cascade, the patient-specific patterns of formation and distribution of intraluminal/intra-prosthetic thrombus formation can be simulated or predicted with acceptable accuracy (Menichini and Xu, 2016; Sun et al., 2021). Based on different thrombus initialization mechanisms, numerous computational models for thrombus formation have been developed in literature (Fogelson, 1992; Wu et al., 2020; Zheng et al., 2020; Bouchnita et al., 2021; Grande Gutiérrez et al., 2021; Méndez Rojano et al., 2022; Shankar et al., 2022). However, the explicit effects of cardiac functions on thrombus formation were not yet well addressed. In order to simulate the coupling between the cardiac function and the hemodynamics environments, we used the lumped parameters-3D coupled models (Kim et al., 2009; Keramati et al., 2022). These models are capable of reflecting the heart function and its effect on the blood flow environment in lumped parameters model with acceptable accuracy in a significantly shorter time. We can use the pressure and velocity profile output from the 0D heart model as inlet conditions for 3D continuum thrombus model. In this pilot study, by coupling a lumped parameters model of cardiac output and aortic/peripheral outflow resistance with a 3D numerical mass transport model of thrombus

formation, we focused on investigating the relation of cardiac functions and the predicted risk of thrombus formation in the aorta and/or endograft of 4 patients who underwent EVAR. Relative risks for thrombus formation were identified using machine-learning algorithms.

Materials and methods

Imaging acquiring and 3D model reconstruction

Four patients diagnosed with AAA who received EVAR and regular follow-ups at the department of vascular surgery of Peking Union Medical College Hospital were included. DICOM format of CTA images of each patient from preoperative and at least 6 months post-operative was obtained. Mimics 12.0 (Materialise, Belgium) and CRIMSON (Arthurs et al., 2021) were used to reconstruct 3D models of the aorta from ascending aorta to aortoiliac bifurcations, with preservation of major branches in the arches and the thoracoabdominal segments (Figure 1A). Models were subsequently smoothed with WRAP (v2017, Geomagic) and loaded into SOLIDWORKS (v18, Solidworks Co.). Vessel outlets were trimmed and extended sufficiently to allow for the fully developed flow pattern. The geometric model was meshed with a tetrahedral mesh using ICEM (v17.0, ANSYS, Inc.). The global meshing size was chosen at .02 mm to accommodate the smallest components. Elements of the boundary layers were set to be hexahedral with a primary thickness of .001 mm and would gradually develop over 5 layers (Figure 1B). Under steady-state conditions, grid independence is considered to be achieved when the mean difference between WSS and platelet concentrations in two continuous simulations is less than 1%. The study followed the Helsinki Declaration and was approved by the ethical committee of Peking Union Medical College Hospital. Written informed consent was obtained from all participants.

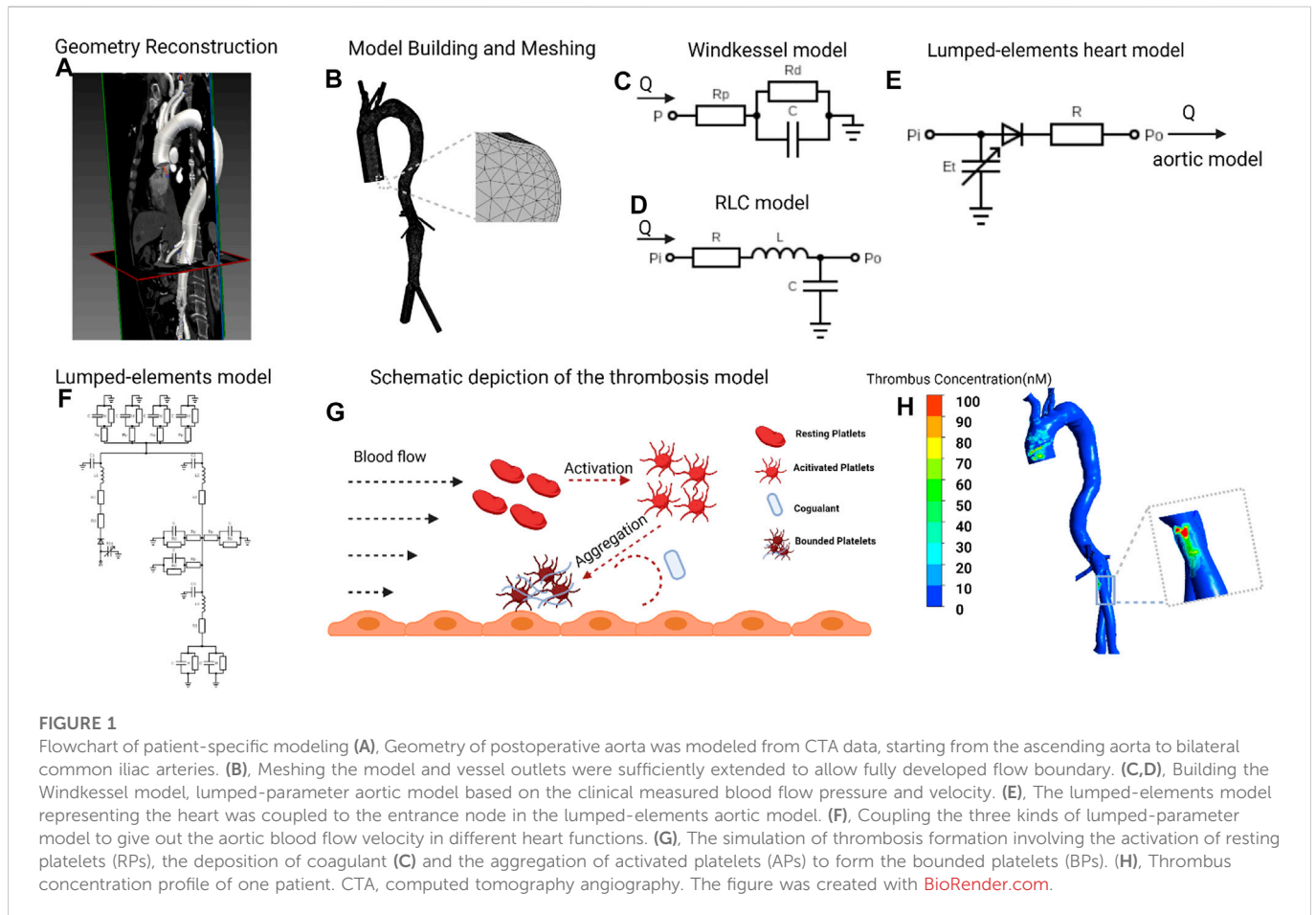
Mathematical modeling for 0D model

The aorta was separated into three sections and represented by three RLC elements. The outlets of the aorta are modeled as the three elements Windkessel model (Westerhof et al., 2009). The parameters in the RLC element and Windkessel model were calculated by solving the differential equations based on the blood flow pressure and velocity. In addition, a function imitating ventricular systole is used in the lumped parameter model of the heart module. Through animal tests, Suga and Sagawa (Suga and Sagawa, 1974) developed a ventricular pressure-volume relationship that can be expressed as a time-varying function $E(t)$, as indicated in Eq. 1:

$$E(t) = \frac{P_{sv}(t)}{V_{sv}(t) - V_0} \quad (1)$$

where $E(t)$ is the time-varying function (mmHg/mL), $P_{sv}(t)$ is the time function of ventricular pressure (mmHg), $V_{sv}(t)$ is a time function of ventricular volume (mL), and V_0 is the ventricular reference volume (mL), which is the theoretical volume relative to ventricular zero pressure. Boston (Goldberger et al., 2000) proposed a mathematical fit to determine the function of ventricular systole according to Eq. 2:

$$E(t) = (E_{max} - E_{min}) \cdot E_n(t_n) + E_{min} \quad (2)$$



where E_{max} refers to the ventricular pressure-volume relation at end-systole, E_{min} refers to the ventricular pressure-volume relation at end-diastolic. $E_n(t_n)$ represents the normalized function of ventricular elasticity, which is described as the Hill equation as follows (Stergiopoulos et al., 1996):

$$E_n(t_n) = 1.55 \left[\frac{\left(\frac{t_n}{0.7}\right)^{1.9}}{1 + \left(\frac{t_n}{0.7}\right)^{1.9}} \right] \left[\frac{1}{1 + \left(\frac{t_n}{1.17}\right)^{1.9}} \right] \quad (3)$$

where t_n is t/T_{max} , and the T_{max} can be calculated from the cardiac cycle:

$$T_{max} = 0.2 + 0.15T \quad (4)$$

Mathematical modeling for 3D simulation of thrombus formation

In this article, we simulate the 3D formation of thrombus by solving the convection-diffusion-reaction equations. The thrombus formation is tracked through the formation of bounded platelets (BPs), which was induced by localized high concentration of activated platelets (APs), coagulation enzymes (C), and prolonged flow residence time (RRT). The schematic of the thrombus formation is illustrated in Figure 1G. We only show the general form of the equation here, and the complete reactions and parameters adapted from the published models (Anand et al., 2003;

Menichini et al., 2016; Sun et al., 2021) are explained in detail in Supplementary Table S2, S3:

$$\frac{\partial [C_i]}{t} + \nabla \cdot (\mathbf{u} \cdot [C_i]) = \nabla \cdot (D_i \cdot \nabla [C_i]) + S_i \# \quad (5)$$

where $[C_i]$ is the concentration of species i ; \mathbf{u} represents the blood flow velocity vector; D_i refers to the diffusivity of species i in blood; and S_i is a local reaction source term for species i . The species considered in this model include resting platelets [RPs], activated platelets [APs], coagulation enzymes [C], and flow residence time [RT].

The bounded platelets (BPs) attached to the reactive surface have neither convective nor diffusive motion; therefore, in this case, Eq. 6 is simplified and the deposition of platelets are governed by the following concentration rate equations:

$$\frac{\partial [C_{BP}]}{t} = S_{BP} \quad (6)$$

where S_{BP} is the local generation rate of bounded platelets (BPs).

Considering the resistance of bounded platelets to blood flow, the momentum source term was added to the Navier-Stokes equations, and the viscosity coefficient was modified. Eq. 7 shows the modified Navier-Stokes equations. and Eqs 8, 9 show the modified viscosity and source term:

$$\rho \frac{\partial \mathbf{u}}{\partial t} + (\mathbf{u} \cdot \nabla) \mathbf{u} = -\nabla p + \mu \Delta \mathbf{u} - S_M \quad (7)$$

TABLE 1 Clinical information and total BP levels of patients under different heart conditions.

	Patient 1	Patient 2	Patient 3	Patient 4	Average
Age, years	80	70	64	83	74.3 ± 7.6
Sex	Male	Female	Male	Male	—
Hypertension	Yes	Yes	Yes	Yes	—
Diabetes	No	Yes	No	No	
Smoking	Yes	No	Yes	No	—
Laboratory results					
LVEF%	68	74	67	77	71.5 ± 4.2
NT-proBNP, pg/mL	104	112	81	77	93.5 ± 14.8
D-dimer, mg/L	6.31	5.3	1.67	1.41	3.7 ± 2.2
HGB, g/L	123	121	150	120	128.5 ± 12.5
Creatinine, μmol/L	78	70	93	111	88.0 ± 15.6
Follow-up, months	35.5	47.7	34.8	11.9	32.5 ± 14.9

BP, bound platelets; E_{max} , maximum elastase; E_{min} , minimum elastase; LVEF, left ventricular ejection fraction. NT-proBNP, NT-proBNP, N-terminal pro-brain natriuretic peptide; HGB, hemoglobin.

$$S_M = k_m \frac{[BP]^2}{[BP]^2 + [BP]_t^2} \mathbf{u} \quad (8)$$

$$\mu = k_\mu \left(1 + \frac{[BP]^2}{[BP]^2 + [BP]_t^2} \right) \quad (9)$$

where ρ represents the blood density equals $1,050 \text{ kg/m}^3$, \mathbf{u} represents the blood flow velocity vector, p represents blood pressure, μ represents the blood viscosity, and S_M represents the local source term of flow momentum. Detailed value of coefficient k_m , k_μ can be found in [Supplementary Material S1 \(Supplementary Table S3\)](#).

Multiscale simulation methods and procedures

Our model coupled the 3D simulation with the lumped-elements model. First, based on the clinically measured blood flow pressure and velocity (Sun et al., 2021), we transformed the aortic model from 3D to lumped elements and coupled the boundary nodes to Windkessel elements (Stergiopoulos et al., 1999) (Figures 1C,D, detailed parameters in [Supplementary Table S1](#)). Subsequently, the lumped-elements model representing the heart was coupled to the entrance node in the lumped-elements aortic model (Figure 1E). We first adjusted the heart model's parameters so that the averaged cardiac output and aortic inlet blood pressure levels matched the clinically determined values. To mimic the various heart functions, we swept the parameters E_{max} (end-systolic elastance), E_{min} (end-diastolic elastance), and T (heart rate) from 10% to -10% compared to the reference values and got the corresponding aortic blood flow velocity in different heart functions. Finally, we simulated the formation of thrombus in the 3D aorta under various cardiac functions, the boundary conditions of which are derived from the blood flow velocity at the boundary nodes in the lumped-elements model (Figures 1F,G). The 3D simulations of blood flow and thrombus formation were performed in FLUENT (v17.0, ANSYS, Inc.) with user-defined functions, whereas the lumped-elements simulations were performed in MATLAB (R2021b, MathWorks, Inc.) The results were analyzed and visualized using CFD-Post (v17.0, ANSYS, Inc.).

Statistical analysis

Data were analyzed using Prism software (v9.0, GraphPad Prism, Inc.). Statistical significance for samples was determined using two-tailed unpaired Student's t-test. Data were considered statistically significant if $p < .05$. The Parallel coordinate analysis and the Multiple correspondence analysis are performed in MATLAB (R2021b, MathWorks, Inc.).

Results

Demographic characteristics and clinical verification of thrombus formation region

The baseline information of 4 patients were shown in [Table 1](#). There were 3 male and 1 female patients, with an average age of 74.3 ± 7.6 years. Pre-operatively, laboratory results indicated normal cardiac and renal function for the 4 subjects. All 4 patients underwent the operation successfully, and follow-up CTA suggested patency of stents and visceral branches. Concerning thrombus formation, CTA results in [Figure 2 \(A1-D1\)](#) illustrated that thrombus was found at the root of the left subclavian artery for patient number 3. For patient number 1, 2, and 4, CTA images all showed thrombus within the iliac stents. Thrombus was not observed at other parts of the arterial or stent model from clinical images. These regions with thrombus formation were defined as the region of interests (ROI) in the following analysis.

The hemodynamic parameters and BP levels at ROI were demonstrated in [Figure 2](#) and [Figure 3](#). The TAWSS, oscillatory shear index (OSI), and relative residence time (RRT) profiles of 4 models were illustrated in [Figure 3](#). In general, TAWSS was highest at the visceral branch level in all 4 patients, which indicated higher frictional force exerted on these vessel areas by the blood flow and prevented activated platelets from binding to coagulant to form thrombus in our model. Descending aorta and iliac branches had higher RRT, which indicated a higher degree of retention for a substance in the bloodstream at the region and induced the development of thrombus in our model (See [Supplementary Material S1](#)). RRT also increased at the oversizing area for the iliac

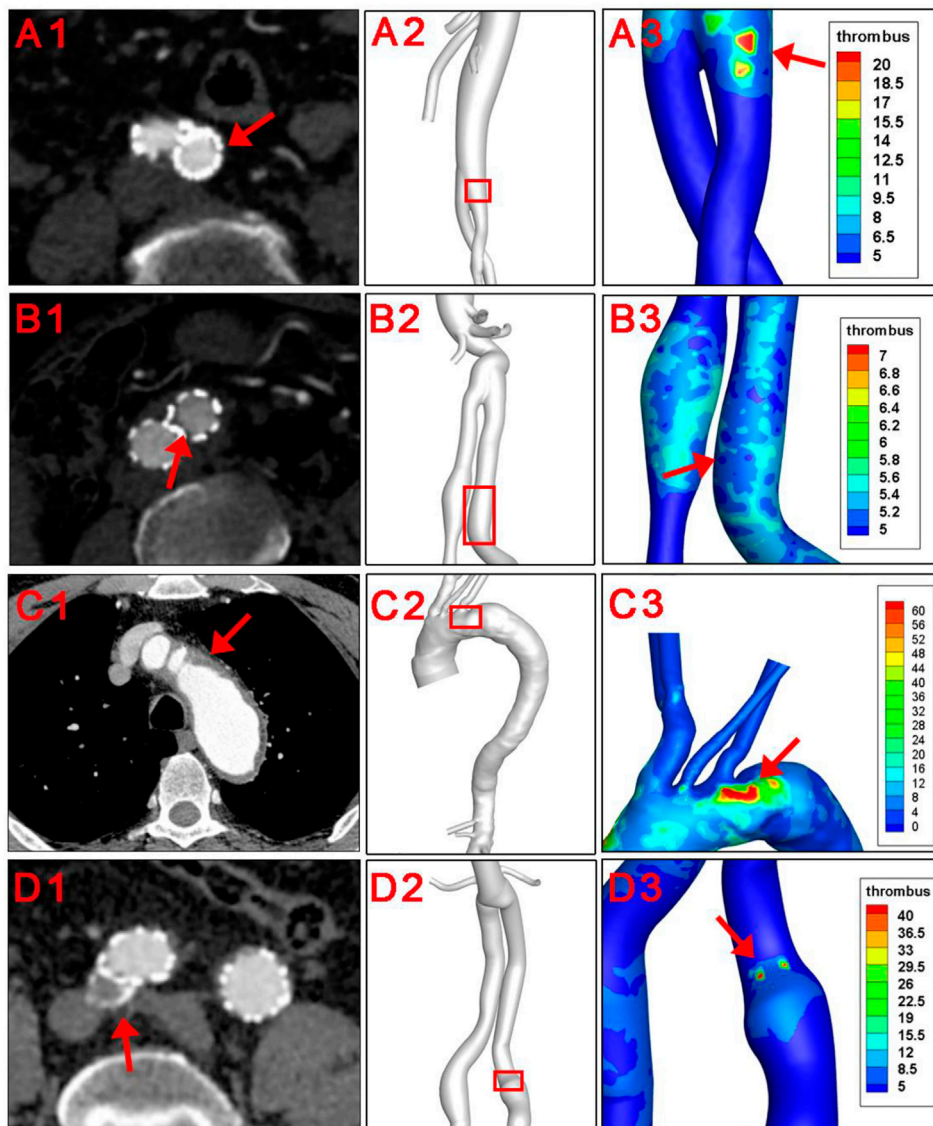


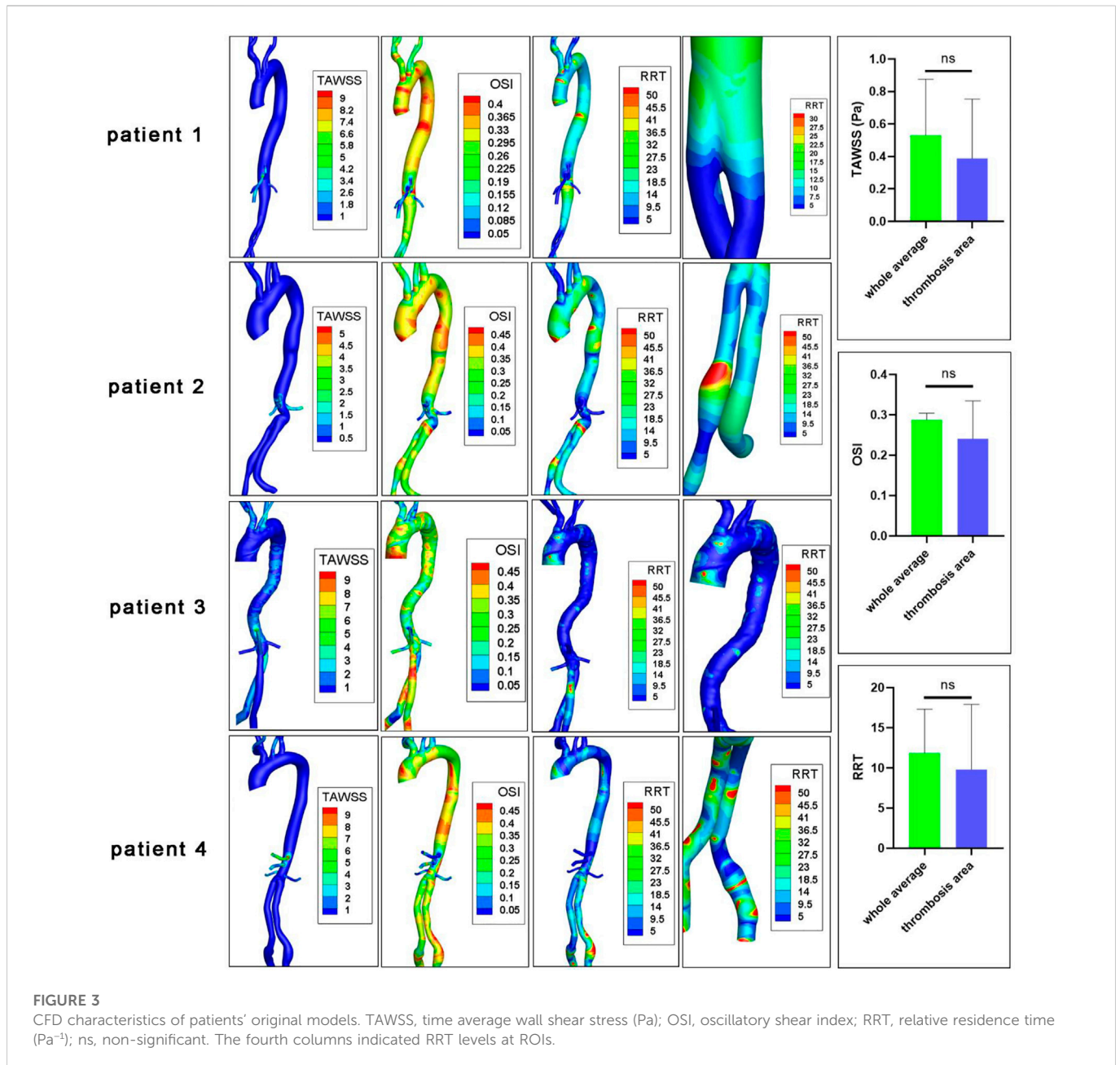
FIGURE 2
Clinical verification of the thrombus forming model. Red arrows and red squares indicated places of thrombus formation on CTA images and corresponding 3D models.

branches. However, zooming in on the ROI in [Figure 2](#) did not indicate distinct abnormal local CFD parameters. In addition, no significant difference in TAWSS, OSI, and RRT was observed for the ROI compared to the average levels of the whole model (right channel in [Figure 3](#)). On the other hand, patterns of BP distribution from the thrombus model simulation [Figure 2](#) (A2–D2) corresponded well with the thrombus results from ROI.

Impact of cardiac function alterations on thrombosis

The impact of heart function alteration on thrombus formation in the ROI as well as the aortic inlet velocity were shown in [Figure 4](#). For patient 1, 2, and 4, the iliac branches were shown, while the arch and descending aorta was illustrated for patient 3.

The aortic velocity profile demonstrated that the magnitude and shape of the blood flow profile are affected by the heart function parameters of E_{max} , E_{min} , and T . Then we analyzed the formation of thrombus, which was induced by the altered heart functions. First of all, the increased E_{max} (end-systolic elastance, representing maximum ventricular contractile force) could maintain or alleviate thrombus formation levels in the ROI of four patients. However, the effects of decreased E_{max} are heterogeneous. For patient 1, a decrease in E_{max} would result in an increase in thrombus development at the iliac branches. However, for patients 2–4, the lower E_{max} would result in less thrombus development at the arch and descending aorta. In addition, the increased E_{min} , which represents ventricular compliance, would maintain or exacerbate the thrombus formation in the ROI of four patients. The decreased E_{min} would maintain or alleviate the thrombus formation in these regions. Furthermore, the influences of heart rate T on thrombus formation are less significant.



We evaluated the area-averaged BP concentration and area-averaged TAWSS (traditional indicator) of the four patients to quantitatively highlight the associations between heart function and thrombus formation in ROI. We discovered that TAWSS is largely affected by E_{max} level, while E_{min} and T have little impact by showing the Parallel coordinate charts classified by the heart function (E_{max} , E_{min} , T ranges from +10% to -10% compared with the reference condition). In addition, we found that increasing E_{max} and decreasing E_{min} could reduce overall thrombus formation levels (Figures 5A, B), which is in agreement with the qualitative analysis. Besides, both the increase and decrease of heart rate T would exacerbate the thrombus formation level (Figure 5C). The effects of E_{min} and t on TAWSS, however, were not significant, indicating the limitations of using hemodynamic features to predict thrombus

development. Then, we performed the multidimensional analysis method to quantitatively reveal the correlations among E_{max} , E_{min} , T , and thrombus formation. We found that the BP concentration was negatively correlated with E_{max} (mean \pm SD: $r = -.2814 \pm .1012$, represents the average correlation coefficient at different segments of the aorta for four patients), and was positively related with E_{min} ($r = .238 \pm .074$) (Figure 5C). However, there was a lack of correlation between heart rate T and BP concentration ($r = -.0148 \pm .1211$). In addition, we found that the ROI (iliac in patient 1,2,4 or arch in patient 3) showed the highest correlations with E_{max} and E_{min} , which indicated that the thrombus formation in these regions was mostly sensitive to the alteration in heart function. Collectively, these data indicated that the increase in E_{max} and decrease in E_{min} would both inhibit thrombus formation, and the effect of T was not significant.

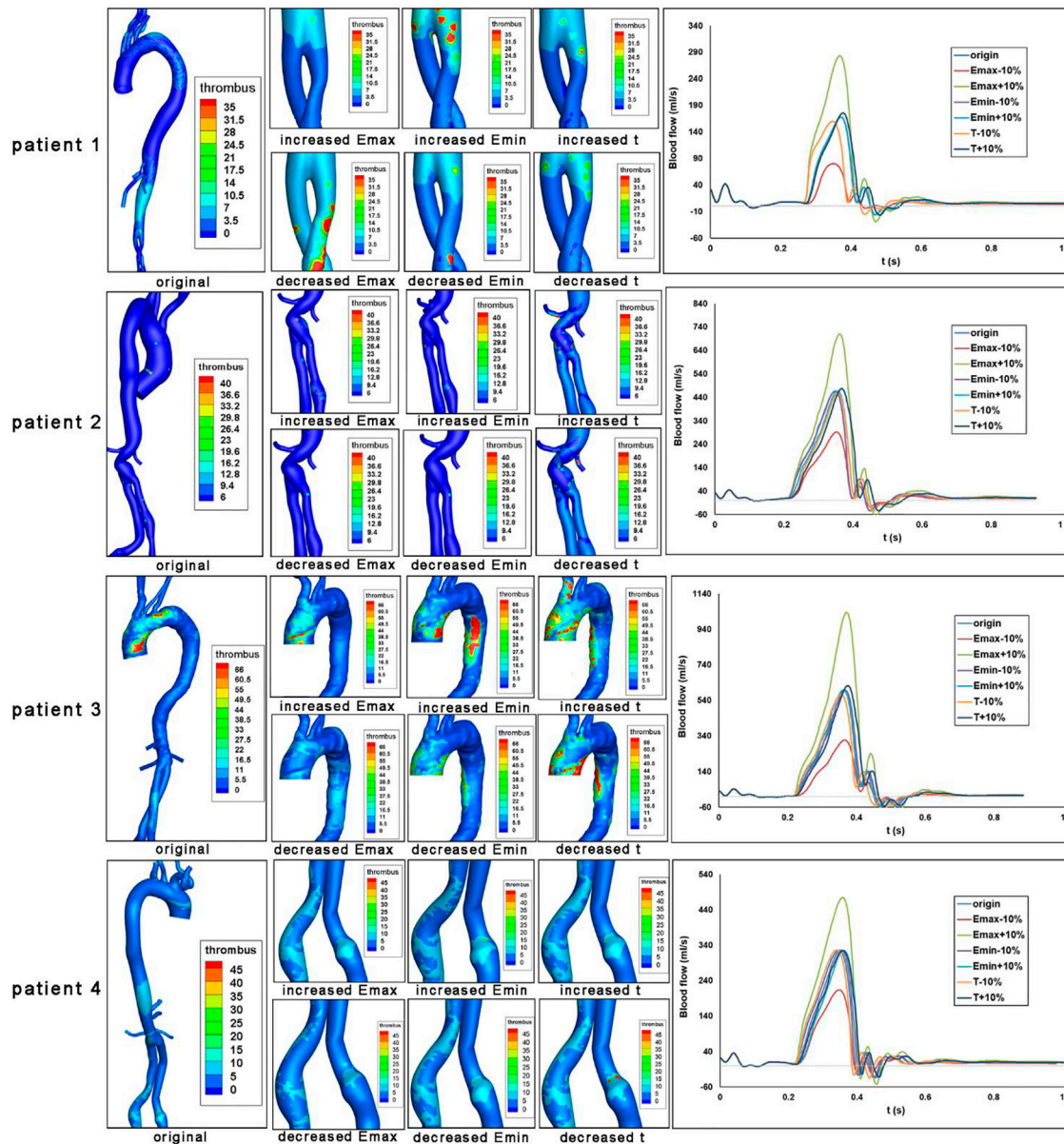


FIGURE 4

Impact of heart function alteration on thrombosis at critical positions. Bounded platelets (BP) levels under different heart conditions were shown for each patient. Aortic blood flow values over a cardiac cycle were also shown.

Discussion

Endograft mural thrombus accumulation had reported rates up to 33% and was detected as early as 1 week after EVAR (Maleux et al., 2008). It might be due to cytokine and prothrombotic factors released from the intramural thrombus of the aneurysm triggered by the operation. Whether the risk of long-term thrombotic events could be increased is debatable (Kapetanos et al., 2018). Mestres et al. reported that endograft mural thrombotic deposits were related to device occlusion during 24 months of follow-up (Mestres et al., 2009), while Melson et al. did not find a significant association (Oliveira et al., 2015). Previous studies on CFD-based thrombus simulation mainly focused on the intra-luminal thrombosis in the sac of AAA. Abnormal wall shear stress, platelet activation, vortical structures, and

morphological parameters were all found to play a potential role (Hansen et al., 2015; Zambrano et al., 2016; Bhagavan et al., 2018; Zambrano et al., 2022). Regarding intra-prothetic thrombosis, Nauta and colleagues investigated the alteration of PLAP in one patient receiving 3 virtual interventions including TEVAR (Nauta et al., 2017). Liu et al. (2021) explored the TAWSS, OSI, and RRT levels in 3 patients who underwent multibranched endovascular repair. Most of these studies referred to previous works or idealized values for boundary blood flow and pressure profiles.

Thrombosis involves complex interlinked interactions between platelets, coagulation cascades, and the vascular wall (Lantz et al., 1981). In this study, traditional hemodynamics parameters including WSS, OSI, and RRT did not precisely identified regions of thrombus formation, probably due to the lack of reflection of this complex

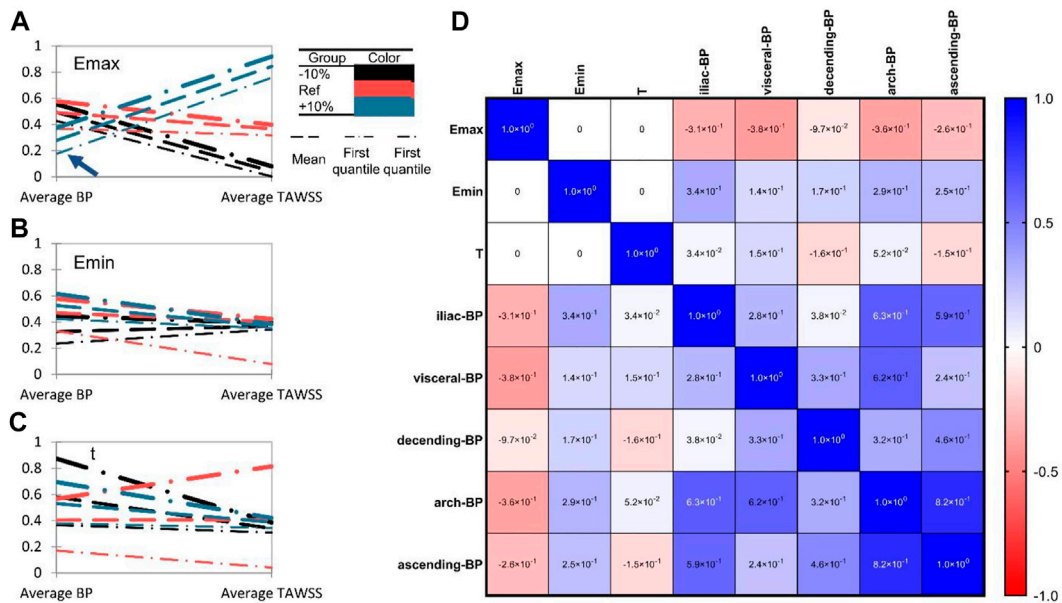


FIGURE 5

Heart function alteration and change of thrombosis or TAWSS at different aortic parts. (A–C). Parallel coordinate charts of BP concentration and TAWSS classified by heart function (E_{max} , E_{min} , T ranges from +10% to –10% compared with the reference state). BP concentration and TAWSS (Pa) have been rescaled ranges from 0 to 1. The arrowhead in (A) indicates the significant role of E_{max} on thrombus formation. (D) Multiple correspondence analysis (MCA) of E_{max} , E_{min} , T, and BP concentration in different aortic sections.

reactions. In a former study, we used a numeric thrombus prediction model to calculate the vascular remodeling and thrombotic events in one patient receiving hybrid repair for the middle aortic syndrome, which was consistent with follow-up images (Sun et al., 2021). The continuum-macroscopic scale model could capture the clotting patterns taking both activated platelets, local hemodynamic conditions, and residence time into account (Menichini and Xu, 2016). Herein, this numeric model was applied to 4 patients receiving EVAR. In line with CTA results, thrombus formation was observed at iliac branches in 3 patients and at the opening of LSCA in 1 patient. Iliac endografts are commonly reported places for thrombosis, and the aorto-uni-iliac configuration was confirmed as a risk factor for intra-prosthetic thrombus (IPT) deposit in a meta-analysis (Perini et al., 2018). The low-density mural thrombus in the descending aorta, on the other hand, may originate from the disruption of vulnerable atherosclerotic plaques (Virmani et al., 2006). Our result suggested that this numeric model was suitable for both intra-luminal and intra-prosthetic thrombosis prediction.

Previous works investigating the relationship between cardiac function and EVAR complications were mainly retrospective cohorts or reviews (Kurzenywyg et al., 2006; Salata et al., 2018). To the best of our knowledge, this is the first attempt at using a cardiac numeric model for post-EVAR patients. Lumped heart models used simple parameters such as resistance and capacitance to simulate the relaxation, filling, contraction, and ejection phases of the heart, and have been widely studied for their interaction with the arterial vessel systems (Hunter et al., 2003). In this study, we used a 0-D cardiac model adapted from Kim et al. to simulate the change in heart function especially ventricular pressure/volume depending on the time-varying elastance curve (Kim et al., 2009). E_{max} represented the maximum ventricular contractility, E_{min} represented ventricular compliance or end-diastolic pressure, and t stood for the cardiac cycle. Heart failure with

reduced ejection fraction (HFREF) or with preserved ejection fraction (HFpEF) could be mimicked under the circumstances. The influence of cardiac parameters on thrombosis was reflected by altered BP levels.

Concerning the actual thrombus forming area, both elevated or reduced E_{min} and t promoted thrombus formation, yet changes of E_{max} induced distinct results. It should be noted that BP levels in patients 1 and 3 were higher and more concentrated around the actual thrombus-forming area. Despite thrombus deposition in the local iliac stent, the BP in patients 2 and 4 had relatively low absolute value and occupied a more extensive spatial range. Morphological factors such as increasing diameter because of stent oversize may have a stronger influence on thrombosis in these patients, and the impact of cardiac parameter alteration should be cautiously interpreted. The heterogeneous results from different patients emphasized the importance of individualized analysis.

Quantitation calculation of BP for general aortic parts revealed that E_{max} was negatively associated with thrombus formation while E_{min} was positively related. It has been reported that male AAA patients had reduced ventricular systolic and diastolic function (Åström Malm et al., 2022). Our result indicated that for patients with CHD (both HFREF and HFpEF) in clinical practice, we should pay more attention to their increased risk of thrombus formation after EVAR. Additionally, preservation of maximum ventricular contractile force and stabilization of ventricular compliance or heart rate was also a crucial consideration when selecting supporting drugs.

This study has some limitations. Patient-specific outflow data of each aortic branch may not always be available, especially for supra-arch branches in AAA patients, and assumptions were made for blood distribution in a limited number of branches according to the literature. The simulation model for thrombus formation could estimate the tendency but not the speed of thrombosis in the vessel model. The simulation process should be applied in a larger patient cohort with multiple follow-up images

to validate our findings. Besides, we ignored the arterial deformation in the 3D calculation. Future studies may combine fluid-structure interaction (FSI) models with mass transport models of thrombus to more realistically predict thrombus formation in deformed vessels (Ma et al., 2021; Chong et al., 2022).

Conclusion

In conclusion, changes in ventricular contractile force may alter the risk of thrombus formation for post-EVAR patients, whereas the effect of heart rate is not significant. Postoperative cardiac support recommends drugs that support maximum ventricular contractile force, maintain left ventricular pressure, and stabilize heart rate.

Data availability statement

The raw data supporting the conclusion of this article will be made available by the authors, without undue reservation.

Ethics statement

The studies involving human participants were reviewed and approved by The ethics committee of Peking Union Medical College Hospital. The patients/participants provided their written informed consent to participate in this study.

Author contributions

XS, ST, YH, YL, and TM led the modelling and calculation of thrombus formation. XS, TM, YZ, and XL conceived, designed, and led the interpretation of the project. XS, ST, RZ and, ZL provides and analyses the clinical data. YC constructed the lumped-elements model. All authors contributed to the writing of the manuscript.

References

- Anand, M., Rajagopal, K., and Rajagopal, K. (2003). A model incorporating some of the mechanical and biochemical factors underlying clot formation and dissolution in flowing blood. *J. Theor. Med.* 5 (3-4), 183–218. doi:10.1080/10273660412331317415
- Arthurs, C. J., Khlebnikov, R., Melville, A., Marčan, M., Gomez, A., Dillon-Murphy, D., et al. (2021). Crimson: An open-source software framework for cardiovascular integrated modelling and simulation. *PLoS Comput. Biol.* 17 (5), e1008881. doi:10.1371/journal.pcbi.1008881
- Åström Malm, I., De Basso, R., Engvall, J., and Blomstrand, P. (2022). Males with abdominal aortic aneurysm have reduced left ventricular systolic and diastolic function. *Clin. physiology Funct. imaging* 42 (1), 1–7. doi:10.1111/cpf.12728
- Banno, H., Kawai, Y., Sato, T., Tsuruoka, T., Sugimoto, M., Kodama, A., et al. (2021). Low-density vulnerable thrombus/plaque volume on preoperative computed tomography predicts for spinal cord ischemia after endovascular repair for thoracic aortic aneurysm. *J. Vasc. Surg.* 73 (5), 1557–1565.e1. doi:10.1016/j.jvs.2020.09.026
- Bhagavan, D., Di Achille, P., and Humphrey, J. D. (2018). Strongly coupled morphological features of aortic aneurysms drive intraluminal thrombus. *Sci. Rep.* 8 (1), 13273. doi:10.1038/s41598-018-31637-6
- Bouchnita, A., Belyaev, A. V., and Volpert, V. (2021). Multiphase continuum modeling of thrombosis in aneurysms and recirculation zones. *Phys. Fluids* 33 (9), 093314. doi:10.1063/5.0057393
- Chong, M. Y., Gu, B., Armour, C. H., Dokos, S., Ong, Z. C., Xu, X. Y., et al. (2022). An integrated fluid-structure interaction and thrombosis model for type B aortic dissection. *Biomechanics Model. Mechanobiol.* 21 (1), 261–275. doi:10.1007/s10237-021-01534-5
- Cunningham, K. S., and Gotlieb, A. I. (2005). The role of shear stress in the pathogenesis of atherosclerosis. *a J. Tech. methods pathology* 85 (1), 9–23. doi:10.1038/labinvest.3700215
- Fogelson, A. L. (1992). Continuum models of platelet aggregation: Formulation and mechanical properties. *SIAM J. Appl. Math.* 52 (4), 1089–1110. doi:10.1137/0152064
- Goldberger, A. L., Amaral, L. A., Glass, L., Hausdorff, J. M., Ivanov, P. C., Mark, R. G., et al. (2000). PhysioBank, PhysioToolkit, and PhysioNet: Components of a new research resource for complex physiologic signals. *circulation* 101 (23), e215–E220. doi:10.1161/01.cir.101.23.e215
- Grande Gutiérrez, N., Alber, M., Kahn, A. M., Burns, J. C., Mathew, M., McCrindle, B. W., et al. (2021). Computational modeling of blood component transport related to coronary artery thrombosis in Kawasaki disease. *PLoS Comput. Biol.* 17 (9), e1009331. doi:10.1371/journal.pcbi.1009331
- Hansen, K. B., Arzani, A., and Shadden, S. C. (2015). Mechanical platelet activation potential in abdominal aortic aneurysms. *J. biomechanical Eng.* 137 (4), 041005. doi:10.1115/1.4029580
- Hunter, P. J., Pullan, A. J., and Smaill, B. H. (2003). Modeling total heart function. *Annu. Rev. Biomed. Eng.* 5, 147–177. doi:10.1146/annurev.bioeng.5.040202.121537
- Isselbacher, E. M., Preventza, O., Black, J. H., 3rd, Augoustides, J. G., Beck, A. W., Bolen, M. A., et al. (2022). ACC/AHA guideline for the diagnosis and management of aortic disease: A report of the American heart association/American College of cardiology joint committee on clinical practice guidelines. *Circulation*.
- Kapetanios, D. M., Karkos, C. D., and Papazoglou, K. O. (2018). Changes in circulating markers of coagulation and fibrinolysis after EVAR. *Int. angiology a J. Int. Union Angiology.* 37 (6), 444–450. doi:10.23736/S0392-9590.18.04046-4

Funding

This work was supported by the National Natural Science Research Foundation of China (Grant No. 11827803, 31971244, 31570947, 32071311, U20A20390, 51890894, 82070492, and 82100519), the Fundamental Research Funds for the General Universities (KG16186101) and the 111 Project (B13003). The CAMS Innovation fund for Medical Science (CIFMS, Grant No. 2021-I2M-C&T-A-006 and 2021-I2M-1-016), and the National High Level Hospital Clinical Research Funding (Grant No. 2022-PUMCH-B-100 and 2022-PUMCH-A-190). The funders had no role in study design, data collection, analysis, decision to publish, or preparation of the manuscript.

Conflict of interest

The authors declare that the research was conducted in the absence of any commercial or financial relationships that could be construed as a potential conflict of interest.

Publisher's note

All claims expressed in this article are solely those of the authors and do not necessarily represent those of their affiliated organizations, or those of the publisher, the editors and the reviewers. Any product that may be evaluated in this article, or claim that may be made by its manufacturer, is not guaranteed or endorsed by the publisher.

Supplementary material

The Supplementary Material for this article can be found online at: <https://www.frontiersin.org/articles/10.3389/fphys.2022.1114110/full#supplementary-material>

- Keramati, H., Birgersson, E., Kim, S., Ho, J. P., and Leo, H. L. (2022). Using a reduced-order model to investigate the effect of the heart rate on the aortic dissection. *Int. J. Numer. Methods Biomed. Eng.* 38, e3596. doi:10.1002/cnm.3596
- Khashram, M., Williman, J. A., Hider, P. N., Jones, G. T., and Roake, J. A. (2016). Systematic review and meta-analysis of factors influencing survival following abdominal aortic aneurysm repair. *Eur. J. Vasc. Endovascular Surg. official J. Eur. Soc. Vasc. Surg.* 51 (2), 203–215. doi:10.1016/j.ejvs.2015.09.007
- Kim, H. J., Vignon-Clementel, I. E., Figueroa, C. A., LaDisa, J. F., Jansen, K. E., Feinstein, J. A., et al. (2009). On coupling a lumped parameter heart model and a three-dimensional finite element aorta model. *Ann. Biomed. Eng.* 37 (11), 2153–2169. doi:10.1007/s10439-009-9760-8
- Kim, W., Gandhi, R. T., Peña, C. S., Herrera, R. E., Scherthaner, M. B., Tsoukas, A., et al. (2017). Effect of β -blocker on aneurysm sac behavior after endovascular abdominal aortic repair. *J. Vasc. Surg.* 65 (2), 337–345. doi:10.1016/j.jvs.2016.06.111
- Kurzenecwyc, D., Filion, K. B., Pilote, L., Nault, P., Platt, R. W., Rahme, E., et al. (2006). Cardiac medical therapy among patients undergoing abdominal aortic aneurysm repair. *Ann. Vasc. Surg.* 20 (5), 569–576. doi:10.1007/s10016-006-9078-z
- Lantz, B. M., Foerster, J. M., Link, D. P., and Holcroft, J. W. (1981). Regional distribution of cardiac output: Normal values in man determined by video dilution technique. *AJR Am. J. Roentgenol.* 137 (5), 903–907. doi:10.2214/ajr.137.5.903
- Lim, S., Halandras, P. M., Park, T., Lee, Y., Crisostomo, P., Hershberger, R., et al. (2015). Outcomes of endovascular abdominal aortic aneurysm repair in high-risk patients. *J. Vasc. Surg.* 61 (4), 862–868. doi:10.1016/j.jvs.2014.11.081
- Liu, M. Y., Jiao, Y., Liu, J., Zhang, S., and Li, W. (2021). Hemodynamic parameters predict in-stent thrombosis after multibranched endovascular repair of complex abdominal aortic aneurysms: A retrospective study of branched stent-graft thrombosis. *Front. Cardiovasc. Med.* 8, 654412. doi:10.3389/fcvm.2021.654412
- Ma, T., Liu, X., Ren, Q., Zhang, Z., Sun, X., Zheng, Y., et al. (2021). Flow-mediated dilation analysis coupled with nitric oxide transport to enhance the assessment of endothelial function. *J. Appl. Physiology* 131 (1), 1–14. doi:10.1152/jappphysiol.00039.2021
- Maleux, G., Koolen, M., Heye, S., Heremans, B., and Nevelsteen, A. (2008). Mural thrombotic deposits in abdominal aortic endografts are common and do not require additional treatment at short-term and midterm follow-up. *J. Vasc. interventional radiology JVIR* 19 (11), 1558–1562. doi:10.1016/j.jvir.2008.08.007
- Méndez Rojano, R., Lai, A., Zhussupbekov, M., Burgreen, G. W., Cook, K., and Antaki, J. F. (2022). A fibrin enhanced thrombosis model for medical devices operating at low shear regimes or large surface areas. *PLOS Comput. Biol.* 18 (10), e1010277. doi:10.1371/journal.pcbi.1010277
- Menichini, C., Cheng, Z., Gibbs, R. G., and Xu, X. Y. (2016). Predicting false lumen thrombosis in patient-specific models of aortic dissection. *J. R. Soc. Interface* 13 (124), 20160759. doi:10.1098/rsif.2016.0759
- Menichini, C., and Xu, X. Y. (2016). Mathematical modeling of thrombus formation in idealized models of aortic dissection: Initial findings and potential applications. *J. Math. Biol.* 73 (5), 1205–1226. doi:10.1007/s00285-016-0986-4
- Mestres, G., Maeso, J., Fernandez, V., Allegue, N., Constenla, I., and Matas, M. (2009). Incidence and evolution of mural thrombus in abdominal aortic endografts. *Ann. Vasc. Surg.* 23 (5), 627–633. doi:10.1016/j.avsg.2008.10.011
- Nauta, F. J. H., Lau, K. D., Arthurs, C. J., Eagle, K. A., Williams, D. M., Trimarchi, S., et al. (2017). Computational fluid dynamics and aortic Thrombus Formation following thoracic endovascular aortic repair. *Ann. Thorac. Surg.* 103 (6), 1914–1921. doi:10.1016/j.athoracsurg.2016.09.067
- Oliveira, N. F., Bastos Gonçalves, F. M., Hoeks, S. E., Ten Raa, S., Ultee, K. H., Rouwet, E., et al. (2015). Clinical outcome and morphologic determinants of mural thrombus in abdominal aortic endografts. *J. Vasc. Surg.* 61 (6), 1391–1398. doi:10.1016/j.jvs.2015.01.032
- Pagoulatou, S., Adamopoulos, D., Rovas, G., Bikiá, V., and Stergiopoulos, N. (2021). The effect of left ventricular contractility on arterial hemodynamics: A model-based investigation. *PLoS one* 16 (8), e0255561. doi:10.1371/journal.pone.0255561
- Perini, P., Bianchini Massoni, C., Azzarone, M., Ucci, A., Rossi, G., Gallitto, E., et al. (2018). Significance and risk factors for intraprostatic mural thrombus in abdominal aortic endografts: A systematic review and meta-analysis. *Ann. Vasc. Surg.* 53, 234–242. doi:10.1016/j.avsg.2018.04.027
- Salata, K., Syed, M., Hussain, M. A., Eikelboom, R., de Mestral, C., Verma, S., et al. (2018). Renin-angiotensin system blockade does not attenuate abdominal aortic aneurysm growth, rupture rate, or perioperative mortality after elective repair. *J. Vasc. Surg.* 67 (2), 629–636. e2. doi:10.1016/j.jvs.2017.09.007
- Saratzis, A., Saratzis, N., Melas, N., and Kiskinis, D. (2008). Pharmacotherapy before and after endovascular repair of abdominal aortic aneurysms. *Curr. Vasc. Pharmacol.* 6 (4), 240–249. doi:10.2174/157016108785909689
- Shankar, K. N., Zhang, Y., Sinno, T., and Diamond, S. L. (2022). A three-dimensional multiscale model for the prediction of thrombus growth under flow with single-platelet resolution. *PLoS Comput. Biol.* 18 (1), e1009850. doi:10.1371/journal.pcbi.1009850
- Stergiopoulos, N., Meister, J.-J., and Westerhof, N. (1996). Determinants of stroke volume and systolic and diastolic aortic pressure. *Am. J. Physiology-Heart Circulatory Physiology* 270 (6), H2050–H2059. doi:10.1152/ajpheart.1996.270.6.H2050
- Stergiopoulos, N., Westerhof, B. E., and Westerhof, N. (1999). Total arterial inertance as the fourth element of the windkessel model. *Am. J. physiology* 276 (1), H81–H88. doi:10.1152/ajpheart.1999.276.1.H81
- Suga, H., and Sagawa, K. (1974). Instantaneous pressure-volume relationships and their ratio in the excised, supported canine left ventricle. *Circulation Res.* 35 (1), 117–126. doi:10.1161/01.res.35.1.117
- Sun, X., Ma, T., Liu, Z., Wu, X., Zhang, B., Zhu, S., et al. (2021). Sequential numerical simulation of vascular remodeling and thrombosis in unconventional hybrid repair of ruptured middle aortic syndrome. *Med. Eng. Phys.* 94, 87–95. doi:10.1016/j.medengphy.2021.06.009
- Virmani, R., Burke, A. P., Farb, A., and Kolodgie, F. D. (2006). Pathology of the vulnerable plaque. *J. Am. Coll. Cardiol.* 47 (8), C13–C18. doi:10.1016/j.jacc.2005.10.065
- Westerhof, N., Lankhaar, J.-W., and Westerhof, B. E. (2009). The arterial windkessel. *Med. Biol. Eng. Comput.* 47 (2), 131–141. doi:10.1007/s11517-008-0359-2
- Wu, W.-T., Zhussupbekov, M., Aubry, N., Antaki, J. F., and Massoudi, M. (2020). Simulation of thrombosis in a stenotic microchannel: The effects of vWF-enhanced shear activation of platelets. *Int. J. Eng. Sci.* 147, 56–72. doi:10.1016/j.ijengsci.2013.12.001
- Zambrano, B. A., Gharahi, H., Lim, C., Jaberi, F. A., Choi, J., Lee, W., et al. (2016). Association of intraluminal thrombus, hemodynamic forces, and abdominal aortic aneurysm expansion using longitudinal CT images. *Ann. Biomed. Eng.* 44 (5), 1502–1514. doi:10.1007/s10439-015-1461-x
- Zambrano, B. A., Gharahi, H., Lim, C. Y., Lee, W., and Baek, S. (2022). Association of vortical structures and hemodynamic parameters for regional thrombus accumulation in abdominal aortic aneurysms. *Int. J. Numer. methods Biomed. Eng.* 38 (2), e3555. doi:10.1002/cnm.3555
- Zheng, X., Yazdani, A., Li, H., Humphrey, J. D., and Karniadakis, G. E. (2020). A three-dimensional phase-field model for multiscale modeling of thrombus biomechanics in blood vessels. *PLoS Comput. Biol.* 16 (4), e1007709. doi:10.1371/journal.pcbi.1007709